Systematic Achievement of Improved Atomic-Scale Contrast
via Bimodal Dynamic Force Microscopy

Shigeki Kawai,* Thilo Glatzel, Sascha Koch, Bartosz Such, Alexis Baratoff, and Ernst Meyer

Department of Physics, University of Basel, Klingelbergstrasse 82, 4056 Basel, Switzerland
(Received 10 December 2008; published 23 November 2009)

Judiciously matched experiments, calculations, and theory demonstrate that a higher sensitivity to short-range interactions and, consequently, improved resolution on the atomic scale can be achieved by bimodal noncontact dynamic force microscopy. The combination of sub-Ångström tip oscillation at the second flexural resonance of a commercially available silicon cantilever with the commonly used large amplitude oscillation at the fundamental resonance frequency enables this performance improvement while avoiding potentially damaging jump-to-contact instabilities.

Since the way to obtain atomically resolved images using frequency-modulation dynamic force microscopy (DFM) was established in 1995 [1], this technique has become a powerful tool [2]. The tip-sample distance is conventionally controlled via the frequency shift Δf_{1st} of the first flexural resonance of a cantilever caused by interaction forces [3]. Atomic-scale contrast arises from short-range forces due to covalent and/or ionic bonding [4,5]. Typically stronger long-range interactions, which depend on the macroscopic tip geometry and the electrostatic potential, act as a background force, but an ultrasharp tip can reduce this contribution. In order to optimize the detection sensitivity of short-range forces, as well as the signal/noise ratio, a small tip oscillation amplitude comparable to the decay length of the short-range interaction (~ 0.1 nm) is desirable [6–8]. A sufficiently high flexural stiffness k_c of the deflection sensor is required to maintain a small amplitude while keeping a stable oscillation. Despite its relatively low mechanical quality factor ($Q \approx 2000$) and low resonance frequency ($f_{1st} \approx 20$ kHz), the tuning fork sensor ($k_c \approx 1800$ N/m) [8,9] used in those pioneering studies [7] has recently been adopted by several groups. Atomic resolution has also been obtained using nonresonant low-frequency excitation in combination with a sensitive interferometric detector [10]. A force sensor with $Q > 10\,000$ and $f_{1st} > 1$ MHz is expected to further enhance spatial resolution [3]. Fortunately, the effective stiffness of higher resonance modes [11] of commercially available cantilevers is high enough to achieve small amplitude operation while satisfying those conditions [12–14].

Using the second flexural mode, stable images have been recorded on the Si(111) surface with amplitudes as small as 70 pm [12,13,15]. In those studies, enhanced sensitivity to short-range interactions due to the small amplitude and a sharp silicon tip enabled imaging at larger tip-sample distances than in conventional DFM. Higher resolution is expected at closer tip-sample distances, i.e., by setting a more negative frequency shift. However, when the closest tip-sample distance in an oscillation cycle becomes comparable to the interatomic spacings, strong attractive forces increases the likelihood of sample and/or tip atom jumps [16]. The resulting force jumps and energy dissipation may prevent stable amplitude control [8]. Moreover, at even smaller closest approach tip-sample distances, the formation and breaking of atomic-scale junctions or necks [17–19] may prevent stable operation. Therefore, stable imaging with small amplitudes at close tip-sample distance is quite challenging, especially on a soft sample surface at room temperature. Recently, frequency vs distance curves without jumps have been measured down to shorter tip-sample distances, albeit using amplitudes larger than about 0.4 nm [14,20].

We circumvented those limitations by simultaneously driving the cantilever at the first f_{1st} and the second flexural resonance frequencies f_{2nd}, with judiciously chosen amplitudes A_{1st} and A_{2nd}, respectively. If $A_{2nd} \ll A_{1st}$, it is theoretically and experimentally demonstrated that Δf_{2nd} is proportional to the force gradient F' averaged over the large oscillation at f_{1st}. Nevertheless, the distance dependence of Δf_{2nd} nearly follows that of F'. The resulting high sensitivity significantly enhances the atomic-scale contrast, while possible instabilities are avoided. Bimodal operation has previously been developed for the amplitude modulation mode in air and liquids, albeit on scales of several to hundreds of nanometers [21–23].

Our experiments were carried out with a DFM setup designed in house [24], which operates at room temperature in ultrahigh vacuum. A clean(001) surface of the KBr sample was obtained by cleaving the crystal in the preparation chamber ($p < 3 \times 10^{-10}$ mbar), then annealing it to remove residual charges. The tip was cleaned by Ar$^+$ sputtering. To obtain atomic resolution, the tip was first gently brought into contact with the surface. The first and second flexural resonance modes of a rectangular silicon cantilever (Nanosensors PPP-NCL, $k_c = 26.5$ N/m) were simultaneously excited with a piezo actuator while keeping preset oscillation amplitudes with automatic gain control-

lers. Δf_{1st} and Δf_{2nd} were demodulated with two independent phase-locked loop (PLL) circuits (Nanonis Dual-OC4). A_{1st} and A_{2nd} were calibrated via the constant frequency shift method [25], using initial amplitudes of 10 nm. The error, which mainly comes from the inaccuracy of the z piezo calibration, was around 10%. The measurements were analyzed using the WSXM software [26].

The steady-state motion of the tip apex in resonant bimodal DFM is adequately described by $z(t) = z_0 + A_{1st}\cos\theta_1 + A_{2nd}\cos\theta_2$, where z_0 is the equilibrium position and $\theta_i = 2\pi f_i t - \phi_i$ the phase of the ith mode. Extending the derivation of Δf_{1st} in conventional DFM [27] to the bimodal case, Δf_{1st} and Δf_{2nd} at the closest approach tip-sample distance ($z_c = z_0 - A_{1st} - A_{2nd}$) can be obtained from

$$A_i k_i \frac{\Delta f_i}{f_i} = \frac{1}{2\pi n_i} \int_0^{2\pi n_i} F[z(t)] \cos\theta_i d\theta_i, \quad (1)$$

where n_i is the (very large) number of oscillation cycles sampled at each recording point, k_i the effective stiffness of the ith mode [11] and $F(z)$ the conservative part of the force acting on the tip. Equation (1) is valid as long as $\Delta f_i/f_i \ll 1$. Harmonic, sum, and difference frequency components of $z(t)$ generated by the nonlinearity of $F(z)$ are then negligible. For $i = 1$ the validity condition prevents cantilever jump-to-contact for large A_{1st}; for $i = 2$ it can be satisfied even for small A_{2nd} provided k_{2nd} is high enough. Because f_{1st} and f_{2nd} are incommensurate, only the force component oscillating at f_i makes a finite contribution to the integral in Eq. (1). Hence the right-hand side is the same when $A_{1st} = A_{2nd}$. On the other hand, if $A_{2nd} \ll A_{1st}$, Δf_{1st} is essentially the same as in conventional DFM, whereas expansion of $z(t)$ in powers of $A_{2nd}\cos\theta_2$ gives a contribution to Δf_{2nd} which averages to zero in leading order. The next order contribution to the integrand, being proportional to $\cos^2\theta_2$ is finite. In the limit $n_2 \to \infty$, incommensurability implies that the θ_2 integration over successive cycles of the oscillation at f_{1st} is equivalent to a dense sampling over a single cycle, and one obtains

$$k_{2nd} \frac{\Delta f_{2nd}}{f_{2nd}} \cong -\frac{1}{4\pi} \int_0^{2\pi} F'(z_0 + A_{1st}\cos\theta_1) d\theta_1. \quad (2)$$

Because $F' = dF/dz$ varies more rapidly than F itself, the short-range contribution to Δf_{2nd} is stronger than to Δf_{1st} in conventional DFM with the same A_{1st}. It is instructive to compare Eq. (2) to the well known small A_{2nd} limit in the absence of simultaneous excitation at f_{1st}, namely

$$\frac{k_{2nd}\Delta f_{2nd}}{f_{2nd}} = -\frac{F'(z_0)}{2}. \quad (3)$$

For this reason, we henceforth *define* the time-averaged F' as $\bar{F}'_i \equiv -2k_i\Delta f_i/f_i$. In order to test these novel results, a simple model based on the Morse potential for the short-range interaction and a Hamaker-type long-range interac-

tion [28] was used. When calculating the latter, the tip radius was set to be 10 nm and the tip-sample distance was offset by 500 pm. Figure 1(a) shows the resulting total interaction $F(z)$ and its $F'(z)$, using the same parameters as in previous studies of Si(111) [4,15].

Figures 1(b)–1(d) show $\bar{F}'_{1st}$ and $\bar{F}'_{2nd}$ numerically calculated over 210 and 1350 oscillation cycles, respectively. As Fig. 1(b) shows that if $A_{1st} = A_{2nd} = 10$ nm, $\bar{F}'_{1st}$ is, as predicted, indistinguishable from $\bar{F}'_{2nd}$. For a smaller $A_{2nd} = 330$ pm the two signals deviate from each other, as shown in Fig. 1(c). Most importantly, the shape of the $\bar{F}'_{2nd}$ curve obtained with an ultrasmall A_{2nd} appears close to that of F', as seen by comparing Figs. 1(a) and 1(d). The maximum value of $\bar{F}'_{2nd}$ is about 6.6 smaller than the maximum value of the gradient, but points calculated from Eq. (2) fall on the curve directly calculated from Eq. (1). Averaging over the oscillation at f_{1st} thus primarily affects the magnitude rather than the distance dependence of $\bar{F}'_{2nd}$.

In order to unambiguously illustrate the improvement in contrast and sensitivity between Δf_{1st} and Δf_{2nd} in bimodal DFM, corresponding images of KBr(001) were recorded in the quasiconstant height mode. The tip-sample distance feedback gains were adjusted such that the topographic corrugation amplitude was below 1 pm, but the slow thermal drift of the tip-sample distance could be compensated. The amplitudes of the first A_{1st} and second flexural modes A_{2nd} were 10 nm and 50 pm, respectively. Figure 2 shows a series of bimodal DFM images at decreasing tip-sample distances, controlled via Δf_{1st} with a step of -2.0 Hz from -14.0 Hz to -20.0 Hz. The bandwidths of the respective frequency demodulators were set at the largest tip-sample distance. Because $A_{2nd} \ll A_{1st}$, the contrast in Δf_{1st} is essentially unaffected by the super-
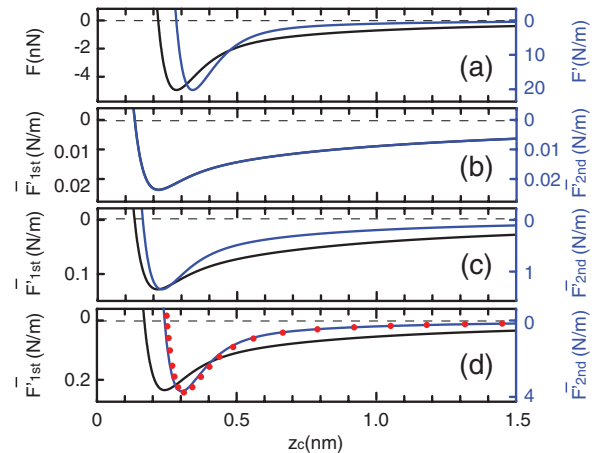
FIG. 1 (color online). Calculated distance dependence of (a) the interaction force F and force gradient F' calculated with the assumed model potential (see text) and of $\bar{F}'_{1st}$ and $\bar{F}'_{2nd}$ with $A_{2nd} = 10$ nm in (b), $A_{2nd} = 330$ pm in (c), and $A_{2nd} = 10$ pm in (d). $A_{1st} = 10$ nm, $f_{1st} = 150$ kHz, and $f_{2nd} = 980$ kHz, in all cases. The points in (d) were calculated using Eq. (2).
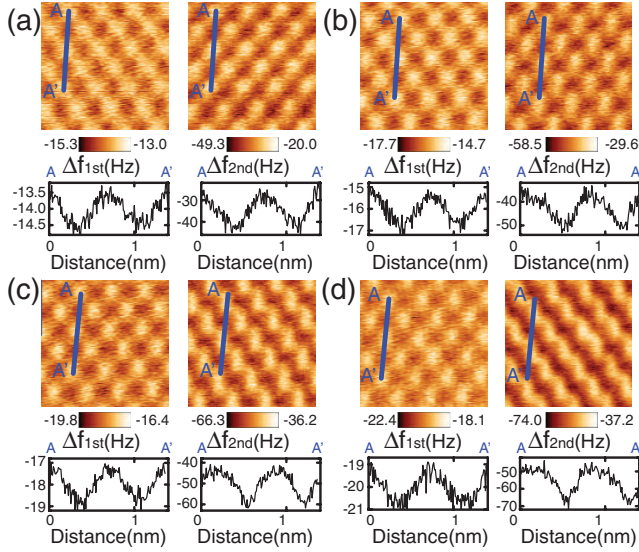
FIG. 2 (color online). Atomically resolved bimodal DFM images of a KBr(001) sample obtained at a series of quasiconstant heights and corresponding line profiles along A-A'. The left and right maps show Δf_{1st} and Δf_{2nd}, respectively. Imaging parameters; (a) $\Delta f_{1st} = -14.0$ Hz, (b) $\Delta f_{1st} = -16.0$ Hz, (c) $\Delta f_{1st} = -18.0$ Hz, and (d) $\Delta f_{1st} = -20.0$ Hz.; $f_{1st} = 154021$ Hz, $A_{1st} = 10$ nm, $Q_{1st} = 31059$, $f_{2nd} = 960874$ Hz, $A_{2nd} = 50$ pm, $Q_{2nd} = 6246$.

posed oscillation at f_{2nd}. Note that in the depicted range, the absolute modulation of Δf_{2nd} is about 10 times stronger than the modulation of Δf_{1st}. This is consistent with the predicted sensitivity enhancement to short-range forces. However, in order to demonstrate contrast improvement it may be more appropriate to compare signal/noise ratios. This is achieved by adjusting the vertical scales in the line profiles are adjusted so that the frequency variations appear the same. Remarkably, the signal-to-noise in Δf_{2nd} becomes better than that in Δf_{1st} as the tip-sample distance is reduced.

At the largest tip-sample distance in Fig. 2(a), the overall observed features in the Δf_{1st} and Δf_{2nd} maps are the same. In Fig. 2(b), the shape of the bright maxima in the Δf_{1st} map does not change, but in the Δf_{2nd} map they appear slightly stretched in the vertical direction. This distortion continuously changed, so that the observed maxima almost merge in [Figs. 2(c) and 2(d)]. Judging from simulations which assumed model KBr tips [29,30], this distortion is mainly due to reversible tip deformations. Comparisons of the magnitude of the computed short-range forces with those extracted from measurements on KBr(001) reported by the same authors strongly suggest that the silicon tip is in fact terminated by a KBr cluster. In our measurements, observed contrast details are indeed sensitive to the tip condition [cf. Figs. 1(d)–1(f) of [31]] and, since the tip apex deforms easier than the surface, tip deformations presumably dominate.

The contrast distortion appears almost exclusively in the Δf_{2nd} map. Together with the comparison of the line profiles, we therefore conclude that the sensitivity to short-range interactions and to induced deformations is significantly higher in Δf_{2nd} than in Δf_{1st} when A_{2nd} is set below 100 pm. Additional evidence for contrast improvement in the topographic mode (constant Δf_{1st}) are provided in [31].

Distant-dependent measurements were performed above a maximum in Fig. 1(d) of Ref. [31]. Figure 3 shows simultaneously recorded variations of Δf_{1st} and Δf_{2nd}. When A_{1st} is equal to A_{2nd}, these two curves have the same shapes, as predicted and shown in Fig. 3(a). The most negative Δf_{1st} and Δf_{2nd} were -17.9 Hz and -1.97 Hz, respectively. Using the measured f_{1st}/f_{2nd} ratio of 6.24, we conclude from Eq. (1) that $k_{2nd}/k_{1st} = 56.7$ in the investigated distance range, i.e., significantly higher than the simple prediction

$$\frac{k_{2nd}}{k_{1st}} \cong \left(\frac{f_{2nd}}{f_{1st}}\right)^2 \cong 40, \qquad (4)$$

valid for a uniform cantilever clamped at one end and free at the other end [11]. An even larger discrepancy was found earlier by comparing two independent Δf_i measurements with separate excitation at f_{1st} and f_{2nd} [14]. The second equality in Eq. (4) was, however, nearly satisfied in those measurements, as well as ours. Since the first equality is assumed in deriving Eq. (1), the higher k_{2nd}/k_{1st} ratios must be attributed to the offset of the tip from the cantilever end, rather than to the relatively small tip mass.

If A_{2nd} is much smaller than A_{1st}, the Δf_{2nd} curve shows a stronger distance dependence than Δf_{1st}, as shown in Fig. 3(b), in agreement with the trend in Figs. 1(b)–1(d).
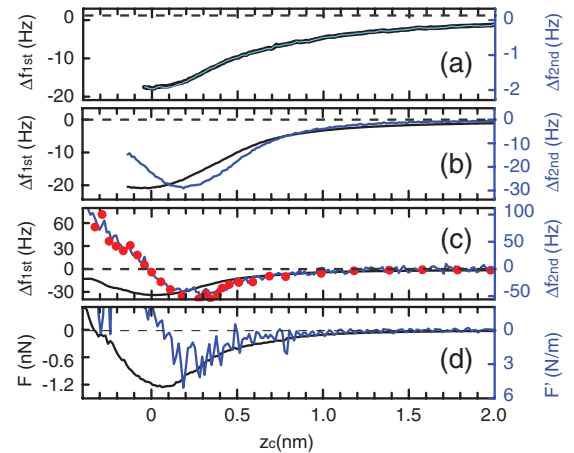
FIG. 3 (color online). Distance dependence of both Δf_{1st} and Δf_{2nd} measured above a maximum in Fig. 1(d) of Ref. [31]: (a) $A_{1st} = 10$ nm and $A_{2nd} = 10$ nm, (b) $A_{1st} = 17.8$ nm and $A_{2nd} = 500$ pm, (c) $A_{1st} = 17.8$ nm and $A_{2nd} = 25$ pm. (d) F calculated from Δf_{1st} in (c) and the corresponding F'. Points in (c) are calculated using Eq. (2). The origin on the horizontal scale being set at the minimum of Δf_{1st} in (c).

With a further decrease of A_{2nd} below 0.1 nm, the detected Δf_{2nd} becomes noisier, and deviates more from Δf_{1st}. When Δf_{1st} reaches its most negative value, Δf_{2nd} is already positive. $F(z)$ was calculated from Δf_{1st} in Fig. 3(c), using Sader's inversion algorithm [32]: Fig. 3(d) shows F and F'. The small noise in $F(z)$ is amplified by the numerical differentiation, but is smoothed out by the integration in Eq. (2). The points in Fig. 3(c), calculated assuming $k_{2nd}/k_{1st} = 56.7$, confirm that Eq. (2) accurately describes the behavior of Δf_{2nd}. The most negative value of Δf_{2nd} predicted by Eq. (3) is too large by a factor ≈ 30, although the shapes of the calculated F' and of Δf_{2nd} curves are rather similar.

For large A_{1st}, by analogy with conventional DFM [27], Δf_{2nd} in Eq. (3) is mainly governed by the short-range variation of F' near the closest turning point of the large oscillation. Δf_{2nd} is then much weaker than without oscillation at f_{1st}, but still large enough to be accurately tracked without having to reduce the scanning speed or to increase the PLL bandwidth, thus keeping detection noise low. A large A_{1st} also allows one to map Δf_{2nd} closer to the surface while avoiding instabilities. In separate measurements of Δf_{2nd} with excitation at f_{2nd} alone, we found that force curves reconstructed from measurements for different A_{2nd} essentially coincide [20], as observed on Si(111)-(7 × 7) [14]. However, tip changes occurred before the most negative Δf_{2nd} could be reached. The threshold A_{2nd} value ensuring stable imaging depended on the tip condition but was significantly larger than 0.1 mm.

In summary, we have demonstrated that stable bimodal DFM can be performed down to closest tip-sample distances in an oscillation cycle where the frequency shift of the second flexural resonance becomes highly sensitive to short-range interactions, thus enhancing the atomic-scale contrast without causing instabilities even on a relatively soft material like KBr. The measurements are in remarkable quantitative agreement with our theoretical predictions.

*shigeki.kawai@unibas.ch

[1] F. J. Giessibl, Science **267**, 68 (1995).
[2] S. Morita, R. Wiesendanger, and E. Meyer, *Noncontact Atomic Force Microscopy* (Springer, Berlin, 2002).
[3] T. R. Albrecht, P. Grütter, D. Horne, and D. Rugar, J. Appl. Phys. **69**, 668 (1991).
[4] R. Pérez, I. Štich, M. C. Payne, and K. Terakura, Phys. Rev. B **58**, 10 835 (1998).
[5] R. Bennewitz, A. S. Foster, L. N. Kantorovich, M. Bammerlin, C. Loppacher, S. Schär, M. Guggisberg, E. Meyer, and A. L. Shluger, Phys. Rev. B **62**, 2074 (2000).
[6] F. J. Giessibl, H. Bielefeldt, S. Hembacher, and J. Mannhart, Appl. Surf. Sci. **140**, 352 (1999).
[7] F. J. Giessibl, S. Hembacher, H. Bielefeldt, and J. Mannhart, Science **289**, 422 (2000).
[8] F. J. Giessibl, Rev. Mod. Phys. **75**, 949 (2003).
[9] F. J. Giessibl, Appl. Phys. Lett. **73**, 3956 (1998).
[10] A. Oral, R. A. Grimble, H. O. Özer, P. M. Hoffmann, and J. B. Pethica, Appl. Phys. Lett. **79**, 1915 (2001).
[11] J. Melcher, S. Hu, and A. Raman, Appl. Phys. Lett. **91**, 053101 (2007).
[12] S. Kawai, S. Kitamura, D. Kobayashi, S. Meguro, and H. Kawakatsu, Appl. Phys. Lett. **86**, 193107 (2005).
[13] S. Kawai, F. Rose, T. Ishii, and H. Kawakatsu, J. Appl. Phys. **99**, 104312 (2006).
[14] Y. Sugimoto, S. Innami, M. Abe, O. Custance, and S. Morita, Appl. Phys. Lett. **91**, 093120 (2007).
[15] S. Kawai and H. Kawakatsu, Appl. Phys. Lett. **88**, 133103 (2006).
[16] L. N. Kantorovich and T. Trevethan, Phys. Rev. Lett. **93**, 236102 (2004).
[17] U. Landman, W. D. Luedtke, N. A. Burnham, and R. J. Colton, Science **248**, 454 (1990).
[18] G. Rubio-Bollinger, P. Joyez, and N. Agraït, Phys. Rev. Lett. **93**, 116803 (2004).
[19] M. A. Lantz, R. Hoffmann, A. S. Foster, A. Baratoff, H. J. Hug, H. R. Hidber, and H.-J. Güntherodt, Phys. Rev. B **74**, 245426 (2006).
[20] S. Kawai, T. Glatzel, S. Koch, B. Such, A. Baratoff, and E. Meyer, Phys. Rev. B **80**, 085422 (2009).
[21] T. R. Rodríguez and R. García, Appl. Phys. Lett. **84**, 449 (2004).
[22] R. García, R. Magerle, and R. Perez, Nature Mater. **6**, 405 (2007).
[23] J. R. Lozano and R. García, Phys. Rev. Lett. **100**, 076102 (2008).
[24] L. Howald, E. Meyer, R. Lüthi, H. Haefke, R. Overney, H. Rudin, and H. J. Güntherodt, Appl. Phys. Lett. **63**, 117 (1993).
[25] G. H. Simon, M. Heyde, and H.-P. Rust, Nanotechnology **18**, 255503 (2007).
[26] I. Horcas, R. Fernandez, J. Gomez-Rodriguez, J. Colchero, J. Gomez-Herrero, and A. Baro, Rev. Sci. Instrum. **78**, 013705 (2007).
[27] F. J. Giessibl and H. Bielefeldt, Phys. Rev. B **61**, 9968 (2000).
[28] M. Guggisberg, M. Bammerlin, C. Loppacher, O. Pfeiffer, A. Abdurixit, V. Barwich, R. Bennewitz, A. Baratoff, E. Meyer, and H. J. Güntherodt, Phys. Rev. B **61**, 11151 (2000).
[29] R. Hoffmann, L. N. Kantorovich, A. Baratoff, H. J. Hug, and H. J. Güntherodt, Phys. Rev. Lett. **92**, 146103 (2004).
[30] K. Ruschmeier, A. Schirmeisen, and R. Hoffmann, Phys. Rev. Lett. **101**, 156102 (2008).
[31] See EPAPS Document No. E-PRLTAO-103-068950 for additional evidence for contrast improvement in the topographic mode (constant Δf_{1st}). For more information on EPAPS, see http://www.aip.org/pubservs/epaps.html.
[32] J. E. Sader and S. P. Jarvis, Appl. Phys. Lett. **84**, 1801 (2004).